



Heat exchange between a bouncing drop and a superhydrophobic substrate

Samira Shiri^a and James C. Bird^{a,1}

^aDepartment of Mechanical Engineering, Boston University, Boston, MA 02215

Edited by William R. Schowalter, Princeton University, Princeton, NJ, and approved May 18, 2017 (received for review January 4, 2017)

The ability to enhance or limit heat transfer between a surface and impacting drops is important in applications ranging from industrial spray cooling to the thermal regulation of animals in cold rain. When these surfaces are micro/nanotextured and hydrophobic, or superhydrophobic, an impacting drop can spread and recoil over trapped air pockets so quickly that it can completely bounce off the surface. It is expected that this short contact time limits heat transfer; however, the amount of heat exchanged and precise role of various parameters, such as the drop size, are unknown. Here, we demonstrate that the amount of heat exchanged between a millimeter-sized water drop and a superhydrophobic surface will be orders of magnitude less when the drop bounces than when it sticks. Through a combination of experiments and theory, we show that the heat transfer process on superhydrophobic surfaces is independent of the trapped gas. Instead, we find that, for a given spreading factor, the small fraction of heat transferred is controlled by two dimensionless groupings of physical parameters: one that relates the thermal properties of the drop and bulk substrate and the other that characterizes the relative thermal, inertial, and capillary dynamics of the drop.

droplets | wetting | heat transfer | microtexture | feathers

An effective method to rapidly cool a surface is to introduce a stream of cold liquid drops, a process referred to as spray cooling (1, 2). Spray cooling is advantageous in applications ranging from electronics (3) to cryogenic dermatology procedures (4). However, there are also situations in which this rapid exchange of thermal energy with droplets is undesirable, such as in ice formation on the wings of an airplane (5), exposure to scalding liquids (6), or heat lost by animals with wet fur and feathers (7, 8). Here, there is an effort to minimize heat exchange by designing superhydrophobic surfaces that can rapidly shed drops from the surface (9–11). Indeed, a drop impacting a superhydrophobic surface can completely bounce, leaving the surface before all possible heat is transferred. However, there is likely some heat exchanged during the short residence time of the drop, and even a small amount of exchanged heat could become significant following aggregate exposure to multiple bouncing drops.

A similar bouncing phenomenon occurs when a drop impacts a surface that is sufficiently hotter than the drop saturation temperature. Under this Leidenfrost or superheated condition, the drop bounces on a cushion of its own vapor (12, 13), preventing direct contact between the solid and liquid and severely limiting the efficacy of spray cooling (14, 15). Models have been developed to predict the partial heat transfer that occurs when drops impact superheated surfaces (16–18); however, it is unclear which aspects of these models, if any, might extend to drops impacting on a superhydrophobic surface when phase change does not occur. In particular, these models typically conclude that the thermal properties of the vapor cushion determine the amount of heat transferred.

Our study addresses how much heat is transferred during the bounce of either a warm or cold water drop on a superhydrophobic substrate in the absence of phase change. Recording the bounce with thermal and high-speed cameras simultaneously enables us to experimentally measure the transferred heat by a single drop over a short residence time. We use can-

dle soot to create a superhydrophobic coating on the substrate, both because it is a simple and effective technique (19, 20) and because the surface properties of soot are highly compatible with thermal imaging. Soot, like other superhydrophobic surfaces, combines chemical hydrophobicity with micro/nanoscale texture, a combination that can support significant air under a water drop (21, 22). The supported air leads to a large effective contact angle and low contact friction, which together cause an impacting drop to rapidly recoil and completely bounce off the surface (23). Indeed, if air escaped from the microstructure, the drop would transition from a Cassie to a Wenzel state, and bouncing would not occur (24). Replacing the vapor layer in previous superheated models (16, 17) with this constant-thickness, air-filled layer predicts the transferred heat Q should scale with initial drop radius R as $Q \sim R^{3.5}$. This scaling is different from the relation that we find for the superhydrophobic surfaces in our experiments, $Q \sim R^{2.75}$.

We propose two different mechanisms that could result in this scaling: one in which the heat transfer is dictated by a cushion of air separating the drop from the superhydrophobic surface and the other in which the heat transfer is based on direct thermal exchange between the drop and the substrate. To discern these mechanisms, we modify the substrate material in our experiments and the subsequent results support the predictions of the direct contact model. We also demonstrate—on a bird feather—an additional model prediction that, for a given flow rate, a superhydrophobic surface can be cooled faster by small drops than by large ones.

Results and Discussion

The heat exchange between a drop and a substrate during a bounce is demonstrated experimentally in Fig. 1. A glass slide is coated with a layer of soot with average thickness $\delta \approx 30 \mu\text{m}$ (Fig. S1). A hot water drop with radius $R = 1.2 \text{ mm}$ and initial

Significance

A superhydrophobic surface can be so water repellent that a drop can bounce off the surface in milliseconds. By measuring the thermal interaction between a superhydrophobic substrate and a heated or cooled drop, we demonstrate that the contact time is short enough that only a small fraction of potential heat is transferred, and, counterintuitively, smaller drops transfer a larger fraction of their potential heat than larger drops despite contacting the surface for less time. Our results indicate that birds with superhydrophobic feathers will be warmer in cold rain than those with feathers on which drops stick, and we envision that a better understanding of these mechanisms can inspire the design of superhydrophobic materials to control heat exchange.

Author contributions: J.C.B. designed research; S.S. performed research; S.S. and J.C.B. analyzed data; and S.S. and J.C.B. wrote the paper.

The authors declare no conflict of interest.

This article is a PNAS Direct Submission.

¹To whom correspondence should be addressed. Email: jbird@bu.edu.

This article contains supporting information online at www.pnas.org/lookup/suppl/doi:10.1073/pnas.1700197114/-DCSupplemental.

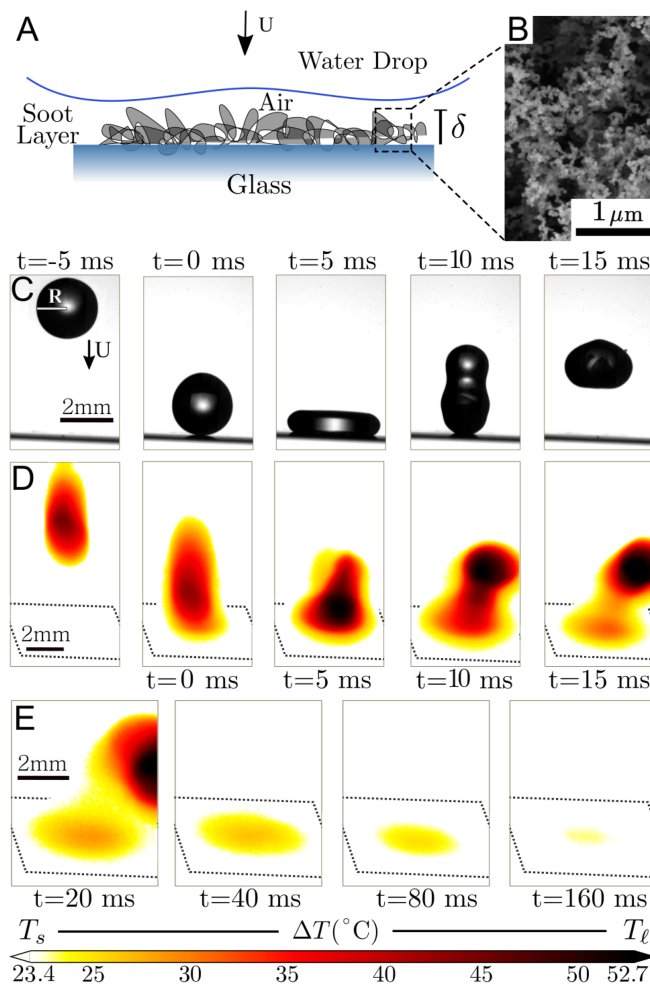


Fig. 1. The finite-time heat exchange between a drop and a superhydrophobic substrate. (A) A water drop impacts a glass substrate coated with a thin layer $\delta \approx 30 \mu\text{m}$ of soot. (B) A scanning electron microscope image of the soot layer reveals the submicrometer roughness responsible for the substrate superhydrophobicity. (C) High-speed images show that the water drop bounces, residing on the surface for a finite time $t_r = 11.8 \text{ ms}$. Here the drop radius is $R = 1.2 \text{ mm}$ and the impact velocity is $U = 0.74 \text{ ms}^{-1}$. (D) Simultaneous thermographic images, from an orthogonal perspective, show a temperature map of the drop surface and substrate during impact. (E) The drop leaves a thermal footprint on the substrate that decays over time. Note that the spatial information from the thermal camera suffers from motion blur due to the 8-ms time response in the uncooled sensor. This exposure time is too long to accurately resolve details during the impact, but is short enough to characterize the thermal footprint left from the drop.

temperature $T_\ell = 52.7^\circ\text{C}$ is released from a suspended needle and impacts, at velocity $U = 0.74 \text{ ms}^{-1}$, a soot-coated glass substrate that is initially at ambient temperature $T_s = 23.4^\circ\text{C}$. Note that the substrate temperature T_s is significantly lower than the saturation temperature for water. Even still, it is possible that the drop might dimple as it nears impact, as has been documented for drops as they approach smooth surfaces (25–27), trapping a cushion of air between the drop and the superhydrophobic surface (Fig. 1A).

When the drop contacts the substrate, the chemistry and sub-micrometer structure of the soot coating (Fig. 1B) repel the water so that the water drop bounces off the surface. The time that the drop resides on the substrate, defined as the residence time t_r , is less than 15 ms (Fig. 1C). Simultaneous thermal images show that the drop leaves the surface before reaching thermal equilibrium (Fig. 1D). The drop leaves a thermal footprint on the

substrate that decays over time (Fig. 1E). Due to the 8-ms time response in the uncooled sensor, there is motion blur during drop impact and recoil that is responsible for the apparent smearing of the drop. However, these motion blur effects are negligible over the longer timescales of the substrate footprint decay used in our analysis.

Further details on the impact dynamics are revealed by plotting the contact radius $r(t)$ as the drop spreads and recoils on the superhydrophobic surface (Fig. 2A). From high-speed images, the contact radius and residence time are extracted for the drop illustrated in Fig. 1. The drop spreads out to a maximum contact radius r_m that is larger than the initial radius of the drop by a spreading factor of $r_m/R = 1.24$. The drop then recoils until it loses contact with the surface at $t_r = 11.8 \text{ ms}$. The maximum contact radius r_m is known to depend on the Weber number $\text{We} \equiv \rho_e U^2 R / \gamma$, a balance of inertial and capillary effects where ρ_e is the liquid density, γ is the surface tension, and U is the impact velocity (28, 29). In this paper, we control the Weber number so that the spreading factor r_m/R is limited to a range between 1.2 and 1.7. In contrast, the residence time is largely independent of the Weber number (23) and instead scales with the inertial-capillary timescale $\sqrt{\rho_e R^3 / \gamma}$. Indeed, the residence time is near the axisymmetric hydrodynamic limit of

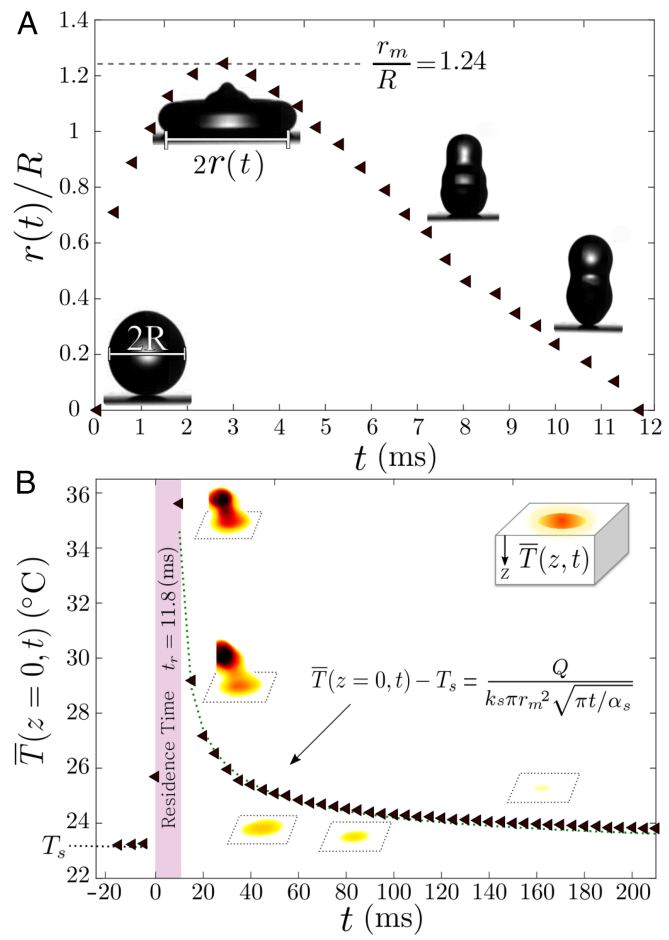


Fig. 2. Extraction of the maximum contact radius r_m and transferred heat Q for the drop illustrated in Fig. 1. (A) Plot of the contact radius $r(t)$ normalized by drop radius R . (B) Average temperature of the drop footprint \bar{T} on the substrate surface ($z = 0$) over time t . The transferred heat Q is calculated by fitting a one-dimensional, semiinfinite heat exchange model (dotted line) as the surface returns to its ambient temperature T_s . Here k_s and α_s are the substrate thermal conductivity and diffusivity, respectively.

$t_r = 2.3 \sqrt{\rho_\ell R^3 / \gamma}$, suggesting that the soot microstructure does not pin the drop as it recedes (30, 31) and is therefore macroscopically equivalent to a drop bouncing on a vapor layer.

As the drop departs the surface, it leaves behind a thermal footprint on the substrate (Fig. 1D), which we use to calculate the transferred heat Q . Immediately after an impact, this heat is concentrated near the substrate surface. We measure the average temperature \bar{T} across the drop contact area for each thermal time-series image, as noted in *Mean Temperature Calculation* (Fig. S2). Plotting this footprint temperature \bar{T} over time t illustrates that the temperature rises rapidly during impact and then returns asymptotically to T_s with a decay rate of ~ 50 ms (Fig. 2B). For the conditions in this experiment, conductive heat transfer is expected to dominate both convective and radiative heat transfer (*Heat Transfer Mechanism*). Additionally, during the first 100 ms after contact, the heat would be expected to diffuse throughout the glass substrate by a distance $\sqrt{\alpha_s t} \approx 210$ μm , where α_s is the thermal diffusivity of the substrate (Table S1). Because this distance is much less than the millimeter thickness of the glass and radius of the footprint, this early-time heat transfer can be approximated as one-dimensional and semiinfinite.

After a pulse of energy, the surface temperature of a semi-infinite, one-dimensional substrate decays in time following the classic self-similar equation

$$\bar{T}(z=0, t) - T_s = \frac{Q}{k_s \pi r_m^2 \sqrt{\pi t / \alpha_s}}, \quad [1]$$

where k_s is the thermal conductivity and πr_m^2 is the contact area over which the energy Q is deposited. For a drop bouncing on a superhydrophobic surface, the energy transfer is not instantaneous; however, the residence time is significantly shorter than the subsequent temperature decay, so the heat transfer can be estimated by fitting Eq. 1 to the average surface temperature in Fig. 2B (dotted line). For the drop shown in Figs. 1 and 2, the estimated heat transferred is $Q = 10$ mJ.

Role of Drop Size and Temperature. To explore the physics underlying the finite-time heat transfer, we carry out a series of experiments in which we systematically vary the drop size R and its initial temperature T_ℓ . In these experiments, we use water as the liquid and soot-coated glass as the substrate. Additionally, we adjust the impact velocity U to constrain the spreading factor to a range between $r_m/R = 1.2$ and 1.7. Repeating the steps illustrated in Figs. 1 and 2, we calculate the transferred heat Q for varying drop sizes R and temperature differences $\Delta T = T_\ell - T_s$ (Fig. 3). To illustrate the effect of the temperature difference ΔT on the transferred heat Q , the data in Fig. 3 are separated into 10°C increments, each of which is represented with a different symbol orientation. Note that ΔT is negative when cold drops, rather than hot drops, impact the superhydrophobic surface. The high-speed optical images allow us to identify the spreading factor r_m/R for each drop, which are separated into 0.1 increments depicted with symbol color and contrast (Fig. 3). As the temperature difference, drop size, and spreading factor increase, the amount of heat transferred increases as well.

A key feature of bouncing drops on superhydrophobic and superheated surfaces is the trapped gas or vapor under the drop. If this gas layer acts as a thermal barrier, we might expect the heat flux to scale with an effective barrier thickness δ . For a given spreading factor, this model would predict the amount of heat transferred to scale as the conduction heat flux across the barrier $\dot{q} \sim k_g \Delta T / \delta$ —where k_g is the thermal conductivity of the confined gas layer—integrated over the contact area $\sim R^2$ for the duration of the residence time $t_r \sim (\rho_\ell R^3 / \gamma)^{1/2}$. Given the importance of the air-filled microscale roughness on the superhydrophobicity, a natural scale for the thickness δ might be the thickness of the superhydrophobic coating itself, which would not vary with drop size or contact time. From a simple scaling per-

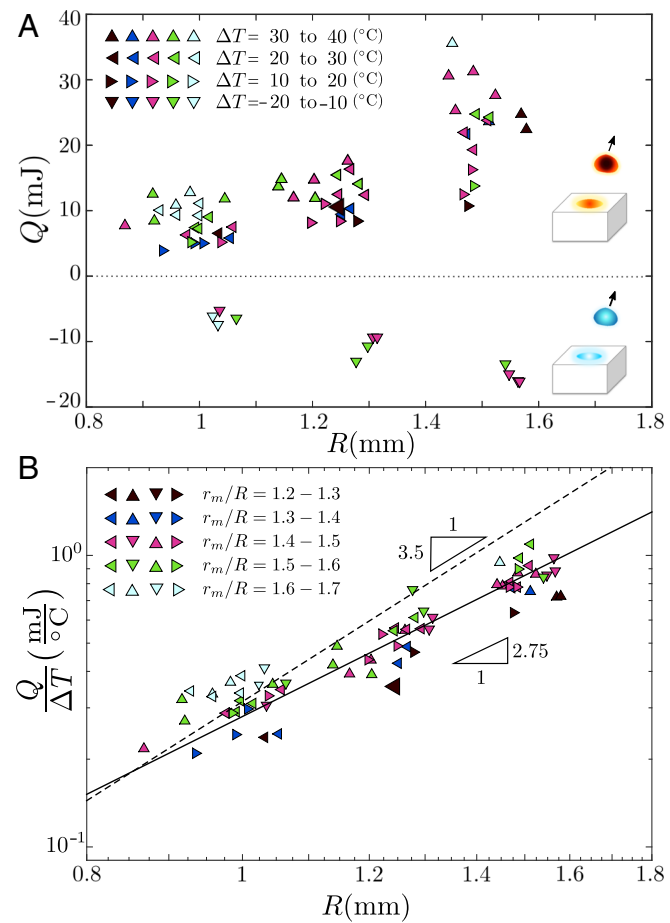


Fig. 3. Measurements of heat transferred by drops. (A) The exchanged heat Q varies with the drop size R ; the temperature difference ΔT between the drop and substrate (symbol orientation); and the extent of spreading, or spreading factor, r_m/R (symbol color). The black arrows illustrate drops bouncing off of the substrate, leaving behind either a warm or cool footprint. (B) The data collapse into single curves for fixed r_m/R when the transferred heat Q is normalized by the initial temperature difference ΔT , showing a power-law dependence on the drop radius R . Note that the larger triangle corresponds to the specific drop illustrated in Fig. 2.

spective, integrating with a constant gap thickness would lead to $Q/\Delta T \sim (k_g/\delta) t_r R^2 \sim (k_g/\delta) (\rho_\ell/\gamma)^{0.5} R^{3.5}$.

An alternative hypothesis is that the trapped gas within the superhydrophobic microtexture has a negligible influence on the heat transfer and that the heat transfer is dominated by the substrate below. In this case, the heat continues to propagate downward into the substrate as the drop spreads and recoils; the characteristic length is self-similar and grows as $\sqrt{\alpha t}$. By substituting this length into the heat flux, we find $Q/\Delta T \sim (k/\sqrt{\alpha t}) t_r R^2 \sim (k/\sqrt{\alpha})(\rho_\ell/\gamma)^{0.25} R^{2.75}$. To evaluate this hypothesis, the experimental results for the transferred heat Q (Fig. 3A) are normalized by the temperature difference ΔT and plotted over a logarithmic scale (Fig. 3B). The data collapse onto a single curve and are more consistent with a power-law scaling of $R^{2.75}$ than $R^{3.5}$.

It is also possible that the heat transfer is dictated by an air cushion above the superhydrophobic surface and that this gap depends on the radius R in such a way to produce a scaling consistent with Fig. 3B. Specifically, research on the trapped air layer over smooth surfaces (32) indicates that the cushion thickness scales as $\delta \sim R(\rho_\ell U R / \mu_g)^{-2/3}$, where μ_g is the viscosity of the air. For a fixed spreading factor, the impact velocity scales as

$U \sim \gamma/\sqrt{\rho R}$, so that $Q/\Delta T \sim (k_g/\delta)t_rR^2 \sim k_g(\rho_\ell\gamma/\mu_g^2)^{1/3}R^{2.8}$. It is noted that the thermal footprint does not reveal any direct evidence of a dimple, such as a lower temperature in the center; nevertheless, both the direct-contact and air-cushion models are consistent with the power-law relationship in Fig. 3B. To adequately discern between these models, we rely on differing predictions for the role of the underlying substrate. In particular, the direct-contact model would be expected to depend on the substrate thermal properties, and a more detailed analysis of this dependence is developed in the next section.

Predicting the Amount of Exchanged Heat. The mechanism of finite-time heat exchange between a drop and a superhydrophobic substrate in the absence of a gas layer and coating can be modeled analytically. Here, we approximate the energy evolution as one dimensional and consider conduction as the main mechanism of heat transfer (*Heat Transfer Mechanism*). If we model the heat flux $\dot{q}(t)$ and contact radius $r(t)$ as decoupled, then the total heat transferred by a single drop over a residence time t_r can be estimated as $Q = \int_0^{t_r} \dot{q}(t)\pi r(t)^2 dt$. The contact radius initially spreads to a maximum radius before retracting back to zero. These spreading and retraction dynamics can be approximated

(1) using the relation $r(t) = 2r_m \sqrt{t/t_r - (t/t_r)^2}$.

To calculate the heat flux $\dot{q}(t)$, we model the drop and substrate as two semiinfinite bodies at different initial temperatures, T_ℓ for the liquid and T_s for the substrate, that are brought into contact and achieve temperature equality at the contact surface, $T(z=0, t)$ (Fig. 4A). For conduction-dominated heat transfer, this semiinfinite approximation is appropriate when the thermal diffusion length $\sqrt{\alpha t_r}$ is less than the thickness of the material. Provided that the drop does not spread too thinly, this condition is met for both the drop and the substrate during their rapid contact.

By imposing the condition that the two bodies have an equal contact temperature during contact time, the standard heat equation can be solved analytically (33), revealing a time-independent contact surface temperature of $T(z=0, t) = (\sqrt{(k\rho c_p)_\ell}T_\ell + \sqrt{(k\rho c_p)_s}T_s)/(\sqrt{(k\rho c_p)_\ell} + \sqrt{(k\rho c_p)_s})$. Here c_p is the specific heat and the subscripts s and ℓ denote the properties of the substrate and liquid, respectively. It follows from the self-similar analysis that the heat flux into the substrate is $\dot{q}(t) = k_s(T_s - T(z=0, t))/\sqrt{\pi\alpha_s t}$. Combining the relations for the heat flux and the contact radius, the amount of heat transferred $Q = \int_0^{t_r} \dot{q}(t)\pi r(t)^2 dt$ is

$$Q = 2.8 \frac{k_s \rho_\ell^{1/4} (r_m/R)^2 \Delta T}{\gamma^{1/4} \sqrt{\alpha_s} \left(1 + \sqrt{(\rho c_p k)_s / (\rho c_p k)_\ell}\right)} R^{11/4}. \quad [2]$$

From a scaling perspective, Eq. 2 is equivalent to the relation $Q/\Delta T \sim R^{2.75}$ presented in the previous section and thus also consistent with the data in Fig. 3A. However, in addition to providing a coefficient, Eq. 2 also provides falsifiable predictions into how the spreading factor and material properties of the liquid and the substrate affect the heat transferred.

A natural way to nondimensionalize the transferred heat Q is to normalize it by the maximum possible heat transfer $m c_p \Delta T$, where m is a drop mass. Noting that $m = \frac{4}{3}\pi R^3 \rho_\ell$, the normalized heat exchange can be expressed as

$$\frac{Q}{m c_p \Delta T} = 0.7 \left(\frac{r_m}{R}\right)^2 \left(\frac{1}{1+\mathcal{M}}\right) \left(\frac{\rho_\ell \alpha_\ell^2}{R\gamma}\right)^{1/4}. \quad [3]$$

In this form, it becomes clear that for a given spreading factor, the model predicts that the fraction of potential heat transferred is controlled by two dimensionless parameters: one relating the thermal-inertial capillary dynamics of the drop $\rho_\ell \alpha_\ell^2 / R\gamma$ and the other relating the thermal properties of the material $\mathcal{M} = k_\ell \sqrt{\alpha_s} / k_s \sqrt{\alpha_\ell}$.

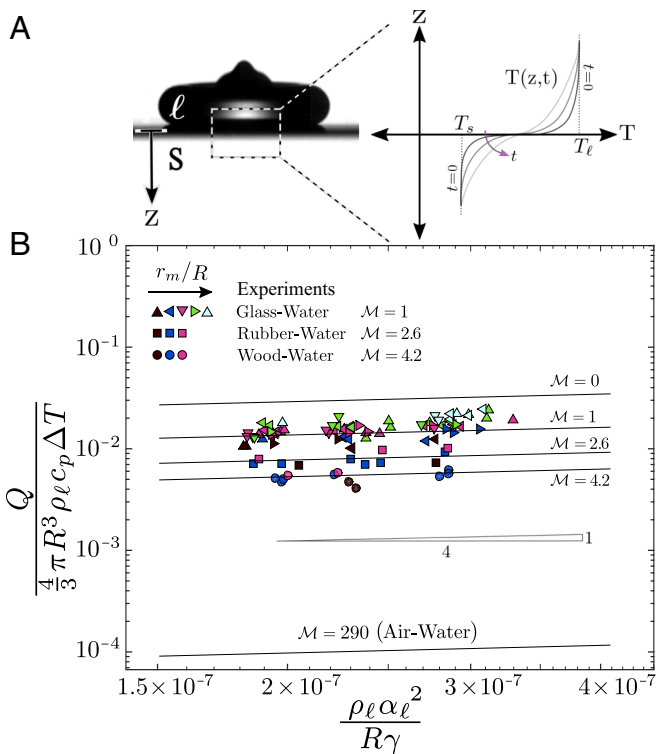


Fig. 4. Comparison between model and experiment. (A) The model assumes that during the residence time t_r , the temperatures of the drop T_ℓ and solid T_s contact along a plane $z=0$ and the heat transfer leads to self-similar temperature profiles $T(z, t)$. (B) For a given spreading factor r_m/R (symbol color), the portion of energy exchanged depends on two dimensionless groups, one based on dynamic properties $\rho_\ell \alpha_\ell^2 / R\gamma$ and the other on material thermal properties \mathcal{M} (symbol shape). The experimental data (symbols) are consistent with the theoretical results with $r_m/R = 1.4$ (solid lines).

The first dimensionless group identified in our analysis, $\rho_\ell \alpha_\ell^2 / R\gamma$, may be interpreted as the square of the ratio of residence time $t_r \sim \sqrt{\rho_\ell R^3 / \gamma}$ to the thermal diffusion time $t_d \sim R^2 / \alpha_\ell$. For millimeter water drops, $\rho_\ell \alpha_\ell^2 / R\gamma$ is of the order of 10^{-7} , which implies that the drop bounces $\sim 2,000$ times faster than the time needed for the heat to thermally diffuse across the drop. The stark difference in timescales supports the semiinfinite approximation. Furthermore, the scaling highlights the competing influence of drop size. A larger drop will have a longer residence time than a smaller drop; yet the increase in diffusion time is greater and therefore the ratio of these timescales t_r/t_d decreases. These two timescales become comparable for sufficiently small drops; yet for water, this size is less than a nanometer or near the molecular scale. Therefore, we would expect $\rho_\ell \alpha_\ell^2 / R\gamma \ll 1$ for most water drops and comparable liquids.

The other control parameter identified in our analysis is the material factor defined as $\mathcal{M} = k_\ell \sqrt{\alpha_s} / k_s \sqrt{\alpha_\ell}$. This factor relates the thermal heat transfer between the liquid and the substrate and therefore depends solely on the thermal properties of these two materials. If the substrate transfers heat significantly faster than the drop, then the heat transfer is rate limited by the drop and $\mathcal{M} \rightarrow 0$; whereas if the substrate transfers heat slower than the drop, then the heat transfer is rate limited by the substrate and $\mathcal{M} \rightarrow \infty$. For a water drop on a glass substrate, the relative heat transfer rates are comparable and $\mathcal{M} = 1$.

The experimental results illustrated in Fig. 3 are rescaled in terms of the dimensionless groups presented in Eq. 3 alongside the theoretical prediction for a spreading factor of $r_m/R = 1.4$

(Fig. 4B). The theoretical model is able to predict not only the scaling trend in the data, but also the prefactor; both experiment and model indicate that ~1% of the available heat is exchanged during the bounce of a millimeter-sized water drop on a superhydrophobic-coated glass substrate. Additionally, as the spreading factor r_m/R is increased, holding the other parameters constant, the amount of heat transferred increases as well, as predicted in the model.

Returning to the two potential models proposed earlier, the direct-contact model depends on the substrate thermal properties, whereas the air-cushion model does not. Specifically, the model predicts that less heat would be exchanged by the bouncing water drop if the glass substrate were replaced by more insulating materials, such as synthetic rubber ($\mathcal{M} = 2.6$) or natural wood ($\mathcal{M} = 4.2$). To test this prediction, we repeat the experimental procedure with neoprene rubber and pine wood instead of glass. The measured thermal properties of these materials are provided in Table S1. A thin superhydrophobic layer of soot is coated on the rubber and wood substrates following the same procedure used for the glass substrate. Thus, the superhydrophobic surfaces in all samples were identical, whereas the underlying substrates differed. Experimental data for heated water drops bouncing on the rubber (square symbols) and wood (circle symbols) are plotted along with the theoretical predictions (Fig. 4B). The results confirm that the substrate material—even under a layer of soot—affects the amount of heat exchanged Q during the drop bounce, providing evidence for the direct-contact model.

An interesting feature of the direct-contact model is that, counterintuitively, a smaller drop can transfer a larger fraction of its potential heat than a larger drop even though the smaller drop is in contact with the surface for less time (Fig. 4B). This result is a consequence of the self-similar conductive heat transfer into the drop and substrate. Indeed, the opposite trend—larger drops transferring a larger fraction of potential heat—would be expected if the heat transfer was regulated by a layer of trapped gas with a fixed depth. These trends are further complicated if the spreading factor r_m/R also varies. Nevertheless, our findings taken at a constant spreading factor (Fig. 4B) illustrate an important concept: Smaller drops may contact the surface for a shorter time than larger drops, yet during this time, the smaller drop encounters a larger average heat flux from the self-similar conduction.

Cooling from Multiple Drops. Although the focus of this paper has been on the heat exchange of individual drops, most applications involve multiple drops. For example, many birds have feathers that are superhydrophobic (7, 21); however, exposure to cold rain can adversely cool a bird (34, 35) and in extreme cases has been linked to hypothermia and death (36, 37).

Our results measuring the small fraction of potential heat exchanged with a drop on a superhydrophobic surface (Fig. 4) suggest that a solid body would be noticeably warmer throughout a cold shower if drops rapidly bounced off the surface rather than becoming stuck. Additionally, these results suggest that at the same flow rate, the bouncing of smaller drops would exchange more heat than that of larger drops, provided that the spreading factor for the smaller drops was similar to or greater than that of the larger drops.

To evaluate these predictions, we measure the temperature T on the underside of a suspended duck feather on top of which a steady stream of drops impacts. These feathers (Fig. 5A) have a barb and barbule microtexture (Fig. 5B) that enables their natural superhydrophobicity. We compare identical experiments on a feather that is superhydrophobic and a feather that has been made superhydrophilic through plasma irradiation (38) and indeed find that the undersides of feathers are warmer when cold droplets bounce rather than stick (Fig. S3).

A superhydrophobic feather can also be used to explore the extent that drop size might affect the amount of heat

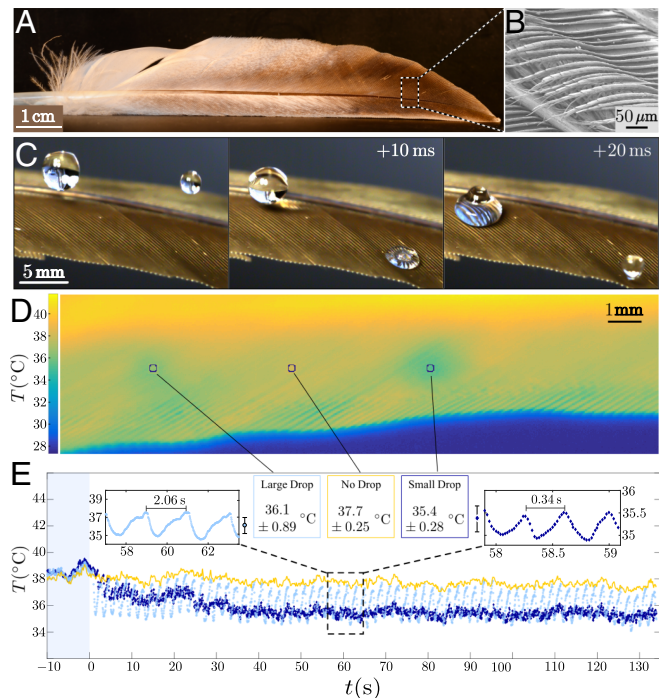


Fig. 5. Cooling from different-sized drops impacting at ambient temperature onto a warmed feather. (A) A photograph of a gray duck pennaceous feather used in the experiments. (B) A scanning electron microscope image reveals the interlocking barb and barbule microtexture that is responsible for the natural superhydrophobicity of the feather. (C) High-speed images show the two different-sized streams of water drops at identical flow rates bounce off of the top surface of the feather. (D) A heat map illustrates the temperature underneath the warmed feather averaged over a 100-s period. During this period, the two streams of ambient-temperature water drops that bounce on the top side of the feather lead, on the bottom side, to local cooling. The circles denote the location of the stream of large drops (left), the stream of small drops (right), and a midpoint in which there are no drops (center). (E) The temperature within each of these circled regions is plotted for 10 s before the start of the experiment, as well as 2 min during which the drops steadily drip on the top side of the feather. Insets highlight the periodicity of the temperature response on the side of the feather opposite to where the drops impact. Here the time between each falling water drop is 2 s for the large drops and 0.3 s for the small drops.

transferred. To explore this possibility, two streams of drops were released simultaneously, one larger ($R \approx 2$ mm) and one smaller ($R \approx 1.1$ mm), with identical flow rates 1 mL/min and similar spreading factors $r_m/R \approx 1.3$ and 1.7, respectively (Fig. 5C). Here the drops were at the ambient laboratory temperature 26 °C, whereas the feather was heated to 40 °C, the approximate body temperature of a bird (39) (Fig. S4).

A time-averaged thermal image from below the feather (Fig. 5D) reveals that the regions under which the large and small drops fall are indeed cooler than the surrounding regions, even though the drops are the same temperature as the ambient air on the top side of the feather. The locations under which the drops fall, as well as the midpoint between these two locations, are denoted with black circles in Fig. 5D. The average temperature within these circled regions varies with time (Fig. 5E). Before the experiment begins ($t < 0$), the temperature within these three regions is indistinguishable. As drops bounce off the feather, the midpoint temperature remains steady whereas the temperature on the opposite side from where the drops fall cools. These temperatures fluctuate, with the region associated with the smaller drop having a lower average temperature than that of the larger drop.

Closer inspection of these temperature fluctuations reveals that they are periodic (Fig. 5E, Insets). Indeed, the period of 2 s for the large drops and 0.3 s for the small drops corresponds precisely with the time interval between the dripping of the large and small drops, respectively, providing additional evidence that the cooling corresponds to the droplet bounce events. Although the cooling from these drops might seem insignificant, it should be noted that the ambient temperature and water drops are relatively warm ($T \approx 26^\circ\text{C}$). More significant temperature drops would be expected in colder conditions. Indeed, identical experiments conducted outdoors in colder weather ($T \approx 3.9^\circ\text{C}$) resulted in significantly greater cooling when the drops bounced on the heated, superhydrophobic feather (Fig. S5).

Conclusion

The findings presented in this study add insight into the finite-time heat transfer that occurs when a hot or cold drop bounces on a superhydrophobic substrate. We demonstrate experimentally and theoretically that a small fraction of available heat is exchanged when a water drop impacts and bounces off a superhydrophobic substrate and that the heat can be modeled as being directly exchanged with the solid substrate. A consequence of this direct exchange is that a greater fraction of available heat is exchanged for smaller than for larger drops, even though larger drops are in contact with the surface for a longer period. Equally significant is the role of the substrate material in the amount of heat exchanged. We highlight how such principles extend to a more general case of multiple bouncing drops and identify dimensionless parameters that can guide the design of nonwetting materials for which heat exchange with impacting drops may be a factor, such as weather-related fabrics. In the context of

avian hypothermia associated with cold rain, past work has indicated that feather water repellency mitigates evaporative cooling (40); our results highlight another important mechanism associated with this process: direct heat exchange with the rain itself.

Materials and Methods

Experimental Methodology. High-speed images are captured using a Photron camera with a frame rate of 10,000 frames per second and a 200-mm Nikon lens. A fiber-optic light source provides cool, high-intensity light to the samples during high-speed imaging. Thermographic images are simultaneously recorded with a thermal camera at a frame rate of 200 frames per second with a close-up IR lens. To control the water temperature, a water bath is connected to a syringe that can eject a single drop on demand. The drop velocity is controlled by varying the height of the needle above the substrate. Velocity adjustments are made to limit the range of the spreading factor r_m/R . In the cooling from the multiple-drops experiments, the feather is suspended by using a stand and clamp. The top of the feather is subjected to two sets of water drops released from two different sizes of needles. A constant flow rate for both sets of drops is maintained with a dual syringe pump. Finally, a heat gun is used to heat the feather from below.

Substrate Material Characterization. To measure the heat capacity of the substrate material, thermal analysis is conducted with a Q2000 differential scanning calorimeter (DSC). The DSC sample measurements are referenced against pure indium metal and evaluated over a range of 15–45 °C, following standard procedures (41). The heat capacity and density of glass, rubber, and wood are measured experimentally and the thermal conductivity values are obtained from the literature (42–44).

ACKNOWLEDGMENTS. We thank J. Goldfarb for assistance in measuring the thermal properties of the solids and K. Varanasi, E. Wang, and F. Brasz for commenting on the manuscript. S.S. acknowledges partial support from the Boston University Dean's Catalyst Award.

1. Leon Bolle JCM (1982) Spray cooling of hot surfaces. *Multiphas Sci Tech* 1:1–97.
2. Kim J (2007) Spray cooling heat transfer: The state of the art. *Int J Heat Fluid Flow* 28:753–767.
3. Deng W, Gomez A (2011) Electrospray cooling for microelectronics. *Int J Heat Mass Tran* 54:2270–2275.
4. Pikkula BM, Torres JH, Tunnell JW, Anvari B (2001) Cryogen spray cooling: Effects of droplet size and spray density on heat removal. *Laser Surg Med* 28:103–112.
5. Thomas SK, Cassoni RP, MacArthur CD (1996) Aircraft anti-icing and de-icing techniques and modeling. *J Aircraft* 33:841–854.
6. McLoughlin E, McGuire A (1990) The causes, cost, and prevention of childhood burn injuries. *Am J Dis Child* 144:677–683.
7. Kennedy R (1970) Directional water-shedding properties of feathers. *Nature* 227:736–737.
8. Voigt CC, Schneeberger K, Voigt-Heucke SL, Lewanzik D (2011) Rain increases the energy cost of bat flight. *Biol Lett* 7:793–795.
9. Mishchenko L, et al. (2010) Design of ice-free nanostructured surfaces based on repulsion of impacting water droplets. *ACS Nano* 4:7699–7707.
10. Patterson CJ, Shiri S, Bird JC (2017) Macrotextured spoked surfaces reduce the residence time of a bouncing Leidenfrost drop. *J Phys Condens Matter* 29:064007.
11. Golovin K, et al. (2016) Designing durable icephobic surfaces. *Sci Adv* 2:e1501496.
12. Burton J, Sharpe A, van der Veen R, Franco A, Nagel S (2012) Geometry of the vapor layer under a Leidenfrost drop. *Phys Rev Lett* 109:074301.
13. Shirotori M, van Limbeek MA, Sun C, Prosperetti A, Lohse D (2016) Dynamic Leidenfrost effect: Relevant time and length scales. *Phys Rev Lett* 116:064501.
14. Leidenfrost JG (1966) On the fixation of water in diverse fire. *Int J Heat Mass Tran* 9:1153–1166.
15. Khavari M, Sun C, Lohse D, Tran T (2015) Fingering patterns during droplet impact on heated surfaces. *Soft Matter* 11:3298–3303.
16. Guo Y, Mishima K (2002) A non-equilibrium mechanistic heat transfer model for post-dryout dispersed flow regime. *Exp Therm Fluid Sci* 26:861–869.
17. Graedech M, Seiler N, Ruyer P, Mailler D (2013) Heat transfer for Leidenfrost drops bouncing onto a hot surface. *Exp Therm Fluid Sci* 47:14–25.
18. van Limbeek MA, et al. (2016) Vapour cooling of poorly conducting hot substrates increases the dynamic Leidenfrost temperature. *Int J Heat Mass Tran* 97:101–109.
19. Bird JC, Mandre S, Stone HA (2008) Short-time dynamics of partial wetting. *Phys Rev Lett* 100:234501.
20. Duez C, Ybert C, Clanet C, Bocquet L (2010) Wetting controls separation of inertial flows from solid surfaces. *Phys Rev Lett* 104:084503.
21. Cassie A, Baxter S (1944) Wettability of porous surfaces. *Trans Faraday Soc* 40:546–551.
22. Koishi T, Yasuoka K, Fujikawa S, Ebisuzaki T, Zeng XC (2009) Coexistence and transition between Cassie and Wenzel state on pillared hydrophobic surface. *Proc Natl Acad Sci USA* 106:8435–8440.
23. Richard D, Clanet C, Quéré D (2002) Surface phenomena: Contact time of a bouncing drop. *Nature* 417:811.
24. Lee C, et al. (2015) Two types of Cassie-to-Wenzel wetting transitions on superhydrophobic surfaces during drop impact. *Soft Matter* 11:4592–4599.
25. Mandre S, Mani M, Brenner MP (2009) Precursors to splashing of liquid droplets on a solid surface. *Phys Rev Lett* 102:134502.
26. van der Veen RC, Tran T, Lohse D, Sun C (2012) Direct measurements of air layer profiles under impacting droplets using high-speed color interferometry. *Phys Rev E* 85:026315.
27. Li E, Thoroddsen ST (2015) Time-resolved imaging of a compressible air disc under a drop impacting on a solid surface. *J Fluid Mech* 780:636–648.
28. Clanet C, Béguin C, Richard D, Quéré D (2004) Maximal deformation of an impacting drop. *J Fluid Mech* 517:199–208.
29. Tran T, Staat HJ, Prosperetti A, Sun C, Lohse D (2012) Drop impact on superheated surfaces. *Phys Rev Lett* 108:036101.
30. Reysset M, Richard D, Clanet C, Quéré D (2010) Dynamical superhydrophobicity. *Faraday Discuss* 146:19–33.
31. Bird JC, Dhiman R, Kwon HM, Varanasi KK (2013) Reducing the contact time of a bouncing drop. *Nature* 503:385–388.
32. Li J, et al. (2016) Oil droplet self-transportation on oleophobic surfaces. *Sci Adv* 2:e1600148.
33. Bergman TL, Incropera FP, DeWitt DP, Lavine AS (2011) *Fundamentals of Heat and Mass Transfer* (Wiley, Hoboken, NJ), 7th Ed.
34. Webb D, King J (1984) Effects of wetting of insulation of bird and mammal coats. *J Therm Biol* 9:189–191.
35. Wilson GR, Cooper SJ, Gessaman JA (2004) The effects of temperature and artificial rain on the metabolism of American kestrels (*Falco sparverius*). *Comp Biochem Physiol A Mol Integr Physiol* 139:389–394.
36. Odum EP, Pitelka FA (1939) Storm mortality in a winter starling roost. *Auk* 56:451–455.
37. Kennedy R (1970) Direct effects of rain on birds: A review. *Br Birds* 63:401–414.
38. Bormashenko E, Grynyov R (2012) Plasma treatment induced wetting transitions on biological tissue (pigeon feathers). *Colloids Surf B Biointerfaces* 92:367–371.
39. Prinzinger R, Pressmar A, Schleucher E (1991) Body temperature in birds. *Comp Biochem Physiol A Physiol* 99:499–506.
40. Lustick S, Adams J (1977) Seasonal variation in the effects of wetting on the energetics and survival of starlings (*Sturnus vulgaris*). *Comp Biochem Physiol A Comp Physiol* 56:173–177.
41. Goldfarb JL, Külaots I (2010) Melting points and enthalpies of fusion of anthracene and its heteroatomic counterparts. *J Therm Anal Calorim* 102:1063–1070.
42. Avallone EA, Baumeister T, III, Sadegh AM (2006) *Marks' Standard Handbook for Mechanical Engineers* (McGraw-Hill, New York), 11th Ed.
43. Ross RJ, et al. (2010) *Wood Handbook: Wood as an Engineering Material* (US Department of Agriculture, Forest Service, Forest Products Laboratory, Madison, WI), Centennial Ed.
44. Perry RH, Green D, Maloney J (1997) *Perry's Handbook of Chemical Engineering* (McGraw-Hill, New York), 7th Ed.